ChemComm

# Multielectron C–H Photoactivation with an Sb(V) Oxo Corrole



| Journal: | *ChemComm* |
|---|---|
| Manuscript ID | CC-COM-12-2019-009892.R1 |
| Article Type: | Communication |
| | |

Chemical Communications

COMMUNICATION

# Multielectron C–H Photoactivation with an Sb(V) Oxo Corrole

Christopher M. Lemon,[†] Andrew G. Maher, Anthony R. Mazzotti, David C. Powers,[‡] Miguel I. Gonzalez, and Daniel G. Nocera*

Received 00th January 20xx,
Accepted 00th January 20xx

DOI: 10.1039/x0xx00000x

www.rsc.org/

**Pnictogen complexes are ideal for mediating multi-electron chemical reactions in two-electron steps. We report a Sb(V) bis-μ-oxo corrole that photochemically oxidises the C–H bonds of organic substrates. In the case of toluene, the substrate is oxidised to benzaldehyde, a rare example of a four-electron photoreaction.**

Nature utilizes the cytochrome P450 family of enzymes to perform a variety of aerobic oxidations including hydrocarbon hydroxylation, alkene epoxidation, and *N*- and *S*-oxidation.[1] Antimony porphyrins have garnered interest as cytochrome P450 mimics,[2–4] owing to similarities between the absorption[5] and magnetic circular dichroism[6] spectra of Sb(III) porphyrins and the CO adduct of cytochrome P450. Augmenting these spectroscopic relationships, antimony porphyrins mediate a variety of photochemical oxidations[7,8] including alkene epoxidation[9,10] and hydrocarbon hydroxylation.[11,12] These reactions demonstrate that main group complexes can serve as alternatives to transition metal catalysts.[13–15]

Though less explored,[16] a photo-oxidation chemistry of Sb corroles is presaged by the similarity to the electronic and redox properties of Sb porphyrins. Enhanced spin-orbit coupling from the Sb centre provides ready access to triplet states.[16] These compounds are efficient singlet oxygen ($^1O_2$) photosensitizers,[17,18] which can be used for the photoinactivation of mould spores[19] and green algae.[20] Other reactions that are prototypical of $^1O_2$ include thioanisole oxidation to the sulfoxide and allylic C–H activation to form the hydroperoxide.[17] Additionally, Sb porphyrins[21] and corroles[22] have been utilized as photosensitizers for bromide oxidation, which occurs via an outer-sphere electron transfer process that is coupled to the two-electron reduction of $O_2$ to $H_2O_2$.

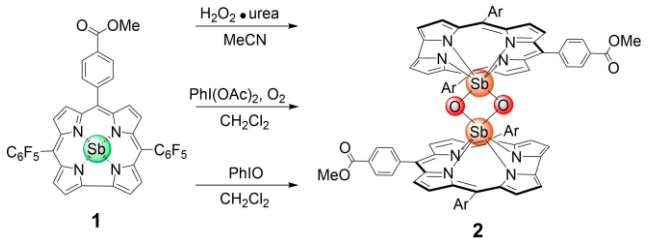


**Figure 1.** Synthesis of the Sb(V) oxo dimer **2** (Ar = $C_6F_5$), which can be prepared using various oxidants: $H_2O_2$ • urea (74% yield), $PhI(OAc)_2/O_2$ (56% yield), or PhIO (71% yield).

As an alternative to manipulating the Sb–X bond by outer-sphere electron transfer, we have developed a direct halogen multielectron photochemistry by exploiting the Sb(III)/Sb(V)$X_2$ couple.[23] This approach complements M–X photoactivation at the $M^{n+2}X_2$ centre of two-electron mixed-valence ($M^n$···$M^{n+2}$) complexes with second- and third-row transition metals.[24–27] Another manifestation of two-electron mixed valency is μ-oxo dimers of first row transition metals bearing macrocyclic ligands.[28] Upon irradiation, the $M^n$–O–$M^n$ moiety is cleaved to generate a $M^{n+1}$=O/$M^{n-1}$ pair; the transient $M^{n+1}$=O performs oxygen atom transfer (OAT) to the substrate. This two-election reactivity has been observed for iron,[29–32] manganese,[33] and ruthenium[34] porphyrins, as well as iron corroles[35,36] and iron phthalocyanines.[37] The analogy between two-electron mixed valence chemistry and pnictogen III/V chemistry suggests that four-electron photochemistry may be achieved with Sb(V) dimers. Here, we present the synthesis and characterization of an Sb(V) bis-μ-oxo corrole dimer and demonstrate that this complex undergoes four-electron photochemistry.

The oxidation of the Sb(III) complex **1** to the Sb(V) derivative was accomplished using three different oxidants (Figure 1). The $^1H$ NMR spectrum of the oxidised product is indicative of a low-symmetry complex, displaying four chemically unique 10-aryl protons at room temperature (see SI). This implies that the antimony centre is out-of-plane and the conformation of the complex is locked, as opposed to the fluxional behaviour of **1** at room temperature.[23] This suggests that the oxidised complex is not a terminal oxo, which would display a $^1H$ NMR spectrum similar to that of **1**. We thus

*Department of Chemistry and Chemical Biology, Harvard University, 12 Oxford St., Cambridge MA 02138, United States*
[†] Present Address: Miller Institute for Basic Research in Science and Department of Molecular and Cell Biology, University of California–Berkeley, Berkeley, CA, 94720
[‡] Present Address: Department of Chemistry, Texas A&M University, College Station, TX, 77843
Electronic Supplementary Information (ESI) available: synthetic methods, experimental details, additional characterisation data, and results from DFT and TD-DFT calculations. See DOI: 10.1039/x0xx00000x

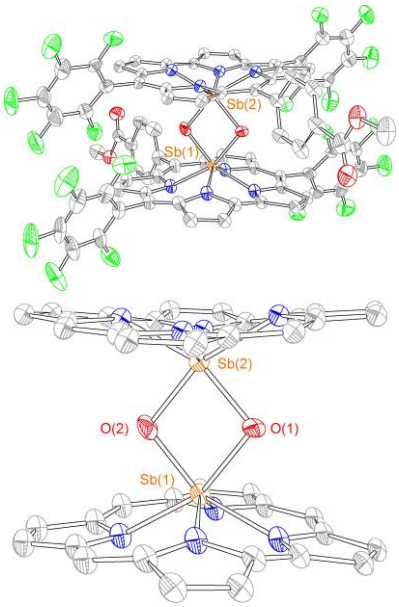


**Figure 2.** Solid-state crystal structure of **2**. Thermal ellipsoids are drawn at the 50% probability level; hydrogen atoms and solvent molecules have been removed for clarity. The *meso* substituents have been removed from the lower structure to better illustrate the Sb coordination geometry.

suspected that the Sb(V) oxo complex of 5,10,15-tris(pentafluorophenyl)corrole, SbO(TPFC),[17] and other corroles,[19,38] which were previously formulated as terminal oxo complexes, are indeed bis-μ-oxo corrole dimers. The geometry of **2** was confirmed by X-ray crystallography (Figure 2, Table S1). Bi(III) halide porphyrins exhibit dimeric structures with two bridging halide anions in a diamond core motif,[39] akin to **2**, further extending the analogy between bismuth porphyrins and antimony corroles.[23] The distance between the Sb centres is long (~3 Å), precluding the formation of a strong Sb···Sb interaction. Similarly, the distance between O atoms is ~2.5 Å, which is longer than typical peroxide and superoxide complexes, indicating the absence of a formal O–O bond.

The cyclic voltammogram of **2** (Figure S1a) exhibits two quasi-reversible oxidations at +0.57 V and +0.76 V vs. $Fc^+/Fc$, as well as an irreversible reduction at –1.49 V with additional irreversible processes observed outside this window. Similarly, SbO(TPFC) exhibits redox processes at +0.65 V and –1.22 V vs. $Fc^+/Fc$.[17] The quasi-reversible waves are attributed to one-electron oxidation of the corrole ligands; this phenomenon is common for cofacial macrocycles that are sufficiently proximate.[40,41] The CV thus supports the notion that the $Sb(V)_2$ bis-μ-oxo core is maintained in solution. For the irreversible reduction process, thin-layer spectroelectrochemistry (Figure S1b) reveals the production of **1**.

The electronic absorption spectrum of **2** (Figure 3) exhibits an intense Soret (or B) band in the near-UV and weaker Q bands in the visible. A pronounced emission band is observed at 610 nm (301 $cm^{-1}$ Stokes shift) with a shoulder at 661 nm. The fluorescence quantum yield of **2** is 0.13% with a corresponding lifetime of <80 ps (within the instrument response function, Figure S2). The fluorescence of **2** is weaker than that of water-soluble Sb(V) oxo corroles ($\phi$ = 2–3%).[19] In

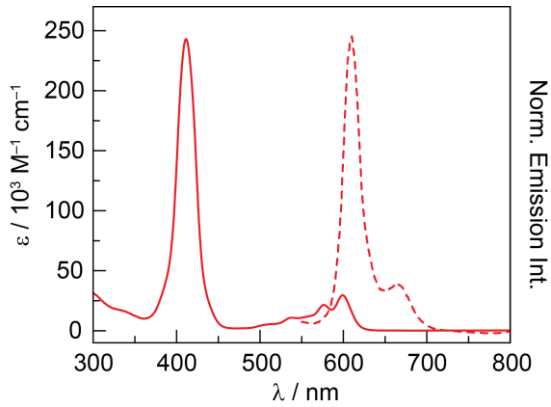


**Figure 3.** Steady-state absorption (solid lines) and emission (dotted lines) spectra of **2** in toluene ($\lambda_{exc}$ = 410 nm).

the absence of a phosphorescence signature, the triplet state was interrogated using nanosecond transient absorption (TA) spectroscopy (Figure S3). Single wavelength kinetics were monitored at 490 nm and the decay followed biexponential kinetics with characteristic lifetimes of $\tau_1$ = 181 ± 9 μs (16%) and $\tau_2$ = 15.7 ± 0.3 μs (84%). The shorter component of the fit[23] is due to the photogeneration of **1** (see below). The triplet lifetime of **2** is consistent with that of SbO(TPFC) (160 μs).[18]

The electronic structure of **2** was examined by DFT and TD-DFT calculations. The geometry of **2** was optimized both as a monomer with a terminal oxo and as a dimer with a bis-μ-oxo diamond core (Figures S4–S8, Tables S2 and S3). The calculated geometry of **2** is consistent with the solid-state structure. The dimeric structure of **2** is 1.503 eV lower in energy than two terminal oxo monomers (+35 kcal/mol for $Sb_2O_2$ (**2**) → 2 Sb=O), indicating that there is a significant driving force for dimerization. Since the TD-DFT calculations of **2** as a dimer did not converge due to the large size of the molecule, these calculations were restricted to the monomer subunits (Figure S9, Tables S4 and S5). The calculated UV-vis spectrum qualitatively corresponds to the experimental spectrum. Three states ($S_5$–$S_7$) were calculated in the 350–380 nm region and correspond to the weak UV bands to the blue of the Soret. In each case, the acceptor orbitals are exclusively LUMO+2 and LUMO+3, which have antibonding character with respect to the Sb–O bond (Figures S10 and S11). Similarly, LUMO+4 and LUMO+7 of **2** are antibonding with respect to the Sb–O bond (Figure S11). Therefore, it is expected that irradiation of **2** ($\lambda_{exc}$ < 375 nm) will populate these orbitals and subsequently result in Sb–O bond activation.

The photochemical reactivity of **2** was studied by irradiating a solution of the compound (3–12 μM) with UV and visible light ($\lambda_{exc}$ > 305 nm) in aerated toluene in the presence of 1,3-cyclohexadiene, a substrate with a weak C–H bond (BDE = 74.3 kcal/mol).[42] Conversion from **2** to **1** was observed, but isosbestic points were not maintained over the course of the reaction, presumably due to $^1O_2$ generation and subsequent decomposition of the corrole. Thus, anaerobic samples were used for all subsequent experiments. Photolysis of **2** in toluene with 1,3-cyclohexadiene maintains isosbestic points for the conversion to **1** (Figure S12a). It should be noted that no conversion to **1** is observed for solutions of **2** stored in the

 

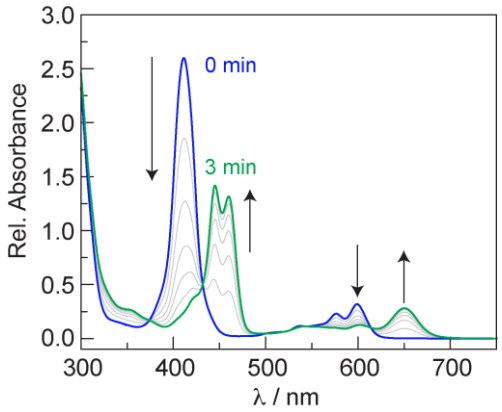


**Figure 4.** Photolysis ($\lambda_{exc}$ > 305 nm) of an anaerobic sample of **2** in toluene. The initial spectrum of **2** (—) evolves to that of **1** (—) over the course of three minutes. Spectra were recorded every 30 sec.

dark. As a control, **2** was irradiated in the absence of diene. However, the conversion of **2** to **1** was facile ($\lambda_{exc}$ > 305 nm), indicating that toluene (BDE($-CH_3$) = 88.5 kcal/mol)[42] also serves as a substrate for C–H activation (Figure 4). As a result, benzene (BDE = 112.9 kcal/mol)[42] was employed as the solvent because it is unreactive under photochemical conditions (Figure S13); conversion of **2** to **1** in benzene with added diene proceeded cleanly (Figure S12b).

A variety of organic substrates, as neat solvents, were evaluated in order to define the limits of **2** to photoactivate C–H bonds. THF (BDE = 92.1 kcal/mol)[42] is a suitable substrate (Figure S14), but acetonitrile (BDE = 96 kcal/mol)[42] is not (Figure S15). Additionally, 2-propanol (BDE = 91 kcal/mol)[42] and cycloheptane (BDE = 94 kcal/mol)[42] were examined using a 1:1 mixture of the substrate and benzene. For 2-propanol, conversion of **2** to **1** is sluggish (Figure S16) and cycloheptane was unreactive (Figure S17). Given these results, we surmise that **2** is able to activate C–H bonds with BDE ≤ 92 kcal/mol under photochemical conditions ($\lambda_{exc}$ > 305 nm).

The photochemical quantum yield for **2** in toluene under monochromatic excitation at 315 nm was 0.18 ± 0.02%. This value is comparable to the quantum yield for toluene activation by a Fe–O–Fe pacman porphyrin ($\phi_{425}$ = 0.15%)[32] and higher than that for a Fe–O–Fe corrole dimer ($\phi_{355}$ = 0.04%).[35] The kinetics for the photogeneration of **1** were monitored by tracking absorbance changes where **2** does not absorb (Figures S18 and S19). Using neat toluene as the substrate, a significant kinetic isotope effect (KIE) is observed (Figure S20). Analysis of three samples, monitoring both 460 nm and 650 nm, gives $k_H$ = 1.25 ± 0.66 × $10^{-8}$ M $s^{-1}$ as compared to $k_D$ = 6.13 ± 1.60 × $10^{-10}$ M $s^{-1}$ when the reaction was performed in toluene-$d_8$ to furnish a KIE = $k_H/k_D$ = 20.4. This value is substantially higher than that for toluene activation by a Fe–O–Fe pacman porphyrin (KIE = 1.55)[32] and ethylbenzene activation by a Fe–O–Fe corrole dimer (KIE = 3.6),[35] indicating that H-atom abstraction (HAA) is fully rate limiting in the case of **2**. Although this KIE also reflects a solvent isotope effect, the large value (>7) suggests that tunnelling is likely occurring.

The organic products from the photochemical reaction in toluene were identified by GC-MS. Neat toluene (9.38 M) was

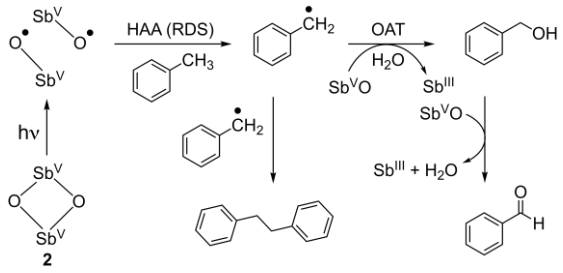


**Figure 5.** Proposed mechanism for the photochemical oxidation of toluene with **2**.

used containing trace amounts of water (~0.03% or 16.6 mM, based on the supplier's specifications). The major products were benzaldehyde and benzyl alcohol, observed in a 14:1 ratio (benzaldehyde to benzyl alcohol); trace amounts of dibenzyl were also observed (Figure S21). This result suggests that the four-electron oxidation prevails. An excess (90–100 equiv) of benzaldehyde was detected relative to the amount of **1** formed during photolysis at high photochemical conversion (40–50%). When anhydrous toluene was used, conversion of **2** to **1** was not observed by absorption spectroscopy and no benzaldehyde was detected by GC-MS. This indicates that water is necessary for the reaction to occur and serves as a proton donor. To exclude water as the primary oxygen source for the organic product, a labelling experiment was performed where dry toluene was saturated with $^{18}O$ water (97 atom %). At low conversion (~3%), only 1.2 equivalents of benzaldehyde were observed per molecule of **1** formed during photolysis. Moreover, the $^{16}O$:$^{18}O$ benzaldehyde product ratio was 9:1, indicating that compound **2** is the primary source of oxygen.

Figure 5 depicts a photochemical reaction sequence that is consistent with the experimental results. The KIE suggests that photon absorption drives HAA from the substrate, shown here to be toluene. The observation of a trace amount of dibenzyl is a consequence of benzyl radical coupling. Formation of the two-electron oxidation product, benzyl alcohol, follows from OAT. A second Sb(V) centre accommodates a second two-electron oxidation to furnish benzaldehyde. Alternatively, the $Sb_2O_2$ core may directly serve as a four-electron oxidant. Given the prevalence of non-innocent corrole complexes,[43,44] the reaction could proceed in one-electron steps with the corrole bearing the redox load to avoid the generation of high-energy Sb(IV) intermediates. Based on the $^{18}O$ experiment, an additional pathway is operative where water serves as the oxygen source. This is also observed under extensive photolysis, where catalytic activity is observed; the amount of product is consistent with the concentration of trace water in the solvent. In this case, the Sb corrole likely serves as a photosensitizer and undergoes a mechanism similar to photochemical oxidations with Sb porphyrins, which utilise water as the O-atom source.[9–12].

Sb(V)-oxo corroles perform multielectron photoredox chemistry. The X-ray structure of **2** represents the first solid-state structure of an Sb(V)-oxo tetrapyrrole. Calculations show that the absorption bands to the blue of the Soret band of **2** populate orbitals that have antibonding character with respect to the Sb–O fragment. Consistent with these calculations,

steady-state photolysis ($\lambda_{exc}$ > 305 nm) of **2** in the presence of a C–H bond with BDE ≤ 92.1 kcal/mol results in conversion to compound **1** with concomitant C–H activation and OAT. Additional experiments with toluene as the substrate indicate that the reaction has a KIE of 20.4. The primary organic product from the photochemical reaction is benzaldehyde: the four-electron oxidation product. This reactivity is in contrast to transition metal M–O–M complexes with macrocyclic ligands, which undergo two-electron photochemical transformations. Based on labelling studies, the oxygen is primarily derived from compound **2**, although oxygen from water is also incorporated, resulting in apparent catalytic benzaldehyde formation. The ability of Sb(V) centres in the oxo complex to work in concert, in much the same way that metal centres in two-electron mixed-valence complexes do, engenders a rare example of a four-electron phototransformation.

This material is based upon work supported by a grant from the National Science Foundation (CHE-1855531). C.M.L. acknowledges the National Science Foundation's Graduate Research Fellowship Program, D.C.P. acknowledges a Ruth L. Kirschstein National Research Service Award (F32-GM103211), and M.I.G. acknowledges the Arnold and Mabel Beckman Foundation for a postdoctoral fellowship. We thank Dr. Sunia Trauger and Jennifer Wang for acquiring mass spectrometry data and Dr. Shao-Liang Zheng for X-ray crystallography assistance. Calculations were performed using the Odyssey cluster supported by FAS Research Computing.

## References

1 B. Meunier, S. P. de Visser and S. Shaik, *Chem. Rev.*, 2004, **104**, 3947–3980.
2 T. Barbour, W. J. Belcher, P. J. Brothers, C. E. F. Rickard and D. C. Ware, *Inorg. Chem.*, 1992, **31**, 746–754.
3 Y. H. Liu, M. F. Bénassy, S. Chojnacki, F. D'Souza, T. Barbour, W. J. Belcher, P. J. Brothers and K. M. Kadish, *Inorg. Chem.*, 1994, **33**, 4480–4484.
4 G. Knör and A. Vogler, *Inorg. Chem.*, 1994, **33**, 314–318.
5 L. K. Hanson, W. A. Eaton, S. G. Sligar, I. C. Gunsalus, M. Gouterman and C. R. Connell, *J. Am. Chem. Soc.*, 1976, **98**, 2672–2674.
6 J. H. Dawson, J. R. Trudell, G. Barth, R. E. Linder, E. Bunnenberg, C. Djerassi, M. Gouterman, C. R. Connell and P. Sayer, *J. Am. Chem. Soc.*, 1977, **99**, 641–642.
7 G. Knör, *Coord. Chem. Rev.*, 1998, **171**, 61–70.
8 T. Shiragami, J. Matsumoto, H. Inoue and M. Yasuda, *J. Photochem. Photobiol. C: Photochem. Rev.*, 2005, **6**, 227–248.
9 H. Inoue, M. Sumitani, A. Sekita and M. Hida, *J. Chem. Soc. Chem. Commun.*, 1987, 1681–1682.
10 H. Inoue, T. Okamoto, Y. Kameo, M. Sumitani, A. Fujiwara, D. Ishibashi and M. Hida, *J. Chem. Soc. Perkin Trans. 1*, 1994, 105–111.
11 T. Shiragami, K. Kubomura, D. Ishibashi and H. Inoue, *J. Am. Chem. Soc.*, 1996, **118**, 6311–6312.
12 S. Takagi, M. Suzuki, T. Shiragami and H. Inoue, *J. Am. Chem. Soc.*, 1997, **119**, 8712–8713.
13 P. P. Power, *Nature*, 2010, **464**, 171–177.
14 C. Weetman and S. Inoue, *ChemCatChem*, 2018, **10**, 4213–4228.
15 R. L. Melen, *Science*, 2019, **363**, 479–484.
16 A. Mahammed and Z. Gross, *Coord. Chem. Rev.*, 2019, **379**, 121–132.
17 I. Luobeznova, M. Raizman, I. Goldberg and Z. Gross, *Inorg. Chem.*, 2006, **45**, 386–394.
18 L. Wagnert, A. Berg, E. Stavitski, I. Luobeznova, Z. Gross and H. Levanon, *J. Porphyrins Phthalocyanines*, 2007, **11**, 645–651.
19 A. Preuß, I. Saltsman, A. Mahammed, M. Pfitzner, I. Goldberg, Z. Gross and B. Röder, *J. Photochem. Photobiol. B, Biol.*, 2014, **133**, 39–46.
20 J. Pohl, I. Saltsman, A. Mahammed, Z. Gross and B. Röder, *J. Appl. Microbiol.*, 2015, **118**, 302–312.
21 M. Ertl, E. Wöß and G. Knör, *Photochem. Photobiol. Sci.*, 2015, **14**, 1826–1830.
22 A. Mahammed and Z. Gross, *Angew. Chem. Int. Ed.*, 2015, **54**, 12370–12373.
23 C. M. Lemon, S. J. Hwang, A. G. Maher, D. C. Powers and D. G. Nocera, *Inorg. Chem.*, 2018, **57**, 5333–5342.
24 A. F. Heyduk and D. G. Nocera, *Science*, 2001, **293**, 1639–1641.
25 T. R. Cook, Y. Surendranath and D. G. Nocera, *J. Am. Chem. Soc.*, 2009, **131**, 28–29.
26 T.-P. Lin and F. P. Gabbaï, *J. Am. Chem. Soc.*, 2012, **134**, 12230–12238.
27 H. Yang and F. P. Gabbaï, *J. Am. Chem. Soc.*, 2014, **136**, 10866–10869.
28 J. Rosenthal, J. Bachman, J. L. Dempsey, A. J. Esswin, T. G. Gray, J. M. Hodgkiss, D. R. Manke, T. D. Luckett, B. J. Pistorio, A. S. Veige and D. G. Nocera, *Coord. Chem. Rev.*, 2005, **249**, 1316–1326.
29 J. M. Hodgkiss, C. J. Chang, B. J. Pistorio and D. G. Nocera, *Inorg. Chem.*, 2003, **42**, 8270–8277.
30 I. M. Wasser, H. C. Fry, P. G. Hoertz, G. J. Meyer and K. D. Karlin, *Inorg. Chem.*, 2004, **43**, 8272–8281.
31 J. Rosenthal, B. J. Pistorio, L. L. Chng and D. G. Nocera, *J. Org. Chem.*, 2005, **70**, 1885–1888.
32 J. Rosenthal, T. D. Luckett, J. M. Hodgkiss and D. G. Nocera, *J. Am. Chem. Soc.*, 2006, **128**, 6546–6547
33 K. W. Kwong, C. M. Winchester and R. Zhang, *Inorg. Chim. Acta*, 2016, **451**, 202–206.
34 R. Zhang, E. Vanover, W. Luo and M. Newcomb, *Dalton Trans.*, 2014, **43**, 8749–8756.
35 D. N. Harischandra, G. Lowery, R. Zhang and M. Newcomb, *Org. Lett.*, 2009, **11**, 2089–2092.
36 R. Zhang, E. Vanover, T.-H. Chen and H. Thompson, *Appl. Catal. A: Gen.*, 2013, **464–465**, 95–100.
37 F. Puls and H.-J. Knölker, *Angew. Chem. Int. Ed.*, 2018, **57**, 1222–1226.
38 S. Mondal, A. Garai, P. K. Naik, J. K. Adha and S. Kar, *Inorg. Chim. Acta*, 2020, **501**, 119300.
39 B. Boitrel, M. Breede, P. J. Brothers, M. Hodgson, L. Michaudet, C. E. F. Rickard and N. Al Salim, *Dalton Trans.*, 2003, 1803–1807.
40 C. J. Chang, Y. Deng, C. Shi, C. K. Chang, F. C. Anson and D. G. Nocera, *Chem. Commun.*, 2000, 1355–1356.
41 Z. H. Loh, S. E. Miller, C. J. Chang, S. D. Carpenter and D. G. Nocera, *J. Phys. Chem. A*, 2002, **106**, 11700–11708.
42 Y. R. Luo, *Handbook of Bond Dissociation Energies in Organic Compounds*, CRC Press, Boca Raton, 2003.
43 A. Ghosh, *Chem. Rev.*, 2017, **117**, 3798–3881.
44 S. Ganguly and A. Ghosh, *Acc. Chem. Res.*, 2019, **52**, 2003–2014.

 